Limit on the mass of a long-lived or stable gluino

G. F. Farrar[a], R. Mackeprang[b], D. Milstead[c], J. P. Roberts[a]

November 15, 2010

[a] *CCPP, New York University, New York, NY 10003, USA*
[c] *Discovery, Center for Particle Physics, Niels Bohr Instititute, Blegdamsvej 17, Copenhagen, Denmark*
[b] *Fysikum, Stockholms Universitet, Stockholm, Sweden*

Abstract

We reinterpret the generic CDF charged massive particle limit to obtain a limit on the mass of a stable or long-lived gluino. Various sources of uncertainty are examined. The R-hadron spectrum and scattering cross sections are modeled based on known low-energy hadron physics and the resultant uncertainties are quantified and found to be small compared to uncertainties from the scale dependence of the NLO pQCD production cross sections. The largest uncertainty in the limit comes from the unknown squark mass: when squark and gluino are degenerate, we obtain a gluino mass limit of 322 GeV, while in the heavy squark limit the gluino mass limit is 397 GeV.

1 Introduction

The observation of exotic stable massive particles (SMPs[1]) which can be detected by their interactions in a detector would be of fundamental significance. SMPs are features of a number of scenarios of physics beyond the Standard Model, such as theories of supersymmetry (SUSY) and extra dimensions [1]. Searches have therefore been carried out at colliders, in cosmic rays and matter [1, 2]. Collider searches for coloured SMPs[2] – R-hadrons in the context of SUSY – present an additional challenge in interpreting the experimental observations, owing to uncertainties in the mass spectra and scattering of the colour-singlet R-hadrons. This is of particular concern for R-hadrons consisting of a heavy colour octet combined with a gluon or $q\bar{q}$ in a colour-octet state, since these systems have no direct analog among Standard Model hadrons [3]. Consequently, there have been no dedicated searches for gluino R-hadrons since the LEP era [4, 5]. In this paper, we outline an approach to model the mass spectra and the scattering of gluino-based R-hadrons which can be used in a search. To preview our method, we reinterpret a recent CDF search [6] to give a lower limit on the mass of a stable or long-lived gluino.

There are two main approaches to searching for strongly interacting SMPs at a collider. One strategy exploits the expected anomalous energy loss of a SMP as it propagates through

[1] The term stable is taken to imply that the particle will not decay during its traversal of a detector.
[2] We will only consider strongly interacting SMPs in the rest of this work and will just use SMP as a shorthand from here on.

an inner tracking system next to the beam-line, while the other relies on the SMP-speed ($\beta \ll 1$) and possible penetrating behaviour whereby a SMP can be measured as a slow-moving object in an outer muon tracking system. Typically, experiments at LEP [4, 5] and HERA [7] exploited the former, while the Tevatron experiments [6, 8] relied on the latter signature. However, since R-hadrons interact hadronically in dense calorimeter material positioned between the aforementioned tracking systems [9, 10, 11], the R-hadron charge can change between the inner detector and when it reaches the outer muon system. The charge of the R-hadron in the outer muon system depends both on the scattering mechanism and the R-hadron mass hierarchies. A comprehensive search for R-hadrons at a collider must consider R-hadron models in which the R-hadron *i)* is dominantly neutral throughout its passage in a detector, *ii)* can be charged in the inner system but is dominantly neutral in the outer tracking systems, and *iii)* can be charged in both the inner and outer trackers. Since the current strongly-interacting SMP-limits from the Tevatron assume the latter scenario, we provide here a gluino mass limit applicable to models which predict the muon-like signature *iii)*.

This paper is organised as follows. First we outline expectations for the gluino-containing R-hadron mass spectra. This is followed by a description of the simulation of R-hadron scattering in matter. Using the material composition of the CDF detector and fixed order QCD-models, the proportions of gluino R-hadrons which would have passed the CDF SMP-selections are then estimated and mass limits extracted.

2 Spectrum of R-hadron masses

To consider the experimental signatures of R-hadrons in a detector we need to postulate a mass spectrum for the R-mesons and the R-baryons. The masses of the R-hadrons have been calculated using the MIT bag model [16] for R-mesons [17] and R-baryons [18][3]. The mass splittings within a given R-hadron multiplet are governed by the same QCD interactions that are responsible for the mass splittings of ordinary mesons and baryons. These are surprisingly well-described by an effective one-gluon-exchange interaction, and many unknown parameters for the R-hadron mass splittings can be fixed by splittings in the analogous ordinary hadrons. To the extent that parameters are determined phenomenologically, splittings should be fairly model-independent.

An important feature of the R-baryon mass spectrum, first pointed out by Farrar [3], is that the lightest R-baryon is the neutral flavor-singlet $u\,d\,s\,\tilde{g}$, denoted S^0. Although the constituent quarks are the same, this is a distinct state from the flavor-octet $\tilde{\Lambda}^0$. Due to the particularly strong hyperfine attraction in the flavor-singlet channel, the S^0 is lighter than the R-proton. There is no flavor-singlet ordinary baryon analog of the S^0, due to Fermi statistics when the quarks form a colour-singlet.

The R-meson spectrum is important for our analysis, because the initial R-hadrons resulting from hadronization of a gluino are predominantly R-mesons. R-mesons are formed by the combination of the gluino with a colour octet $q\overline{q}$ pair. We must also consider the gluino-ball $\tilde{g}g$ on a similar footing as it mixes directly with the flavor singlet R-meson states. The states can be broken down by first considering the $q\overline{q}$ state and then combining this with the spin-$\frac{1}{2}$ $\tilde{g}$. The combination of the $J^C = 0^-$ $q\overline{q}$ state with the $1/2^-$ gluino gives a $1/2^+$ R-meson. The combination of the 1^+ $q\overline{q}$ state with the gluino gives both a $1/2^-$ nonet and a $3/2^+$ nonet.

[3] Lattice calculations have been performed for R-mesons and gluino-balls, e.g., [19], but the bag-model results are consistent with the lattice calculations and easier to use.

It is sufficient to focus only on the lightest states so we simplify the meson sector to include the two lightest nonets with $J = 1/2$. In [17] it is shown that as $m_{\tilde{g}} \to \infty$, the mass splitting between states becomes constant: $m_{\tilde{K}} - m_{\tilde{\rho}} = 130$ MeV, $m_{\tilde{\pi}} - m_{\tilde{\rho}} = 40$ MeV. It is important that the R-pions ($1/2^+$) are *not* significantly lower in mass than other non-strange R-mesons, unlike the ordinary pions, because they are not pseudo-Goldstone bosons. Thus we take the R-meson masses to be split only by the strange quark content[4]. With two light nonets and a gluino-ball we have 19 states: 10 degenerate non-strange R-mesons, a gluino-ball we take to be degenerate, and a heavier set of 8 R-kaons. We take the mass splitting between these states to be 130 MeV. For ease of reference we refer to all non-strange R-mesons as $\tilde{\pi}$ from here on, and all strange R-mesons as $\tilde{K}$.

$m_{\tilde{K}} - m_{\tilde{\pi}}$	130 MeV

Table 1: The mass splitting of the R-meson states stable against strong decays from [17].

In the R-baryon sector the gluino combines with a qqq colour octet. The qqq state can have either $J = 1/2$ or $J = 3/2$; combined with the spin-1/2 gluino this gives a set of states with $J = 0, 1, 2$. Fermi statistics requires that the $J = 3/2$ qqq state be a flavour octet, while the $J = 1/2$ state can be a flavour singlet, octet or decuplet. Buccella et al [18] showed that for gluino masses above 1 GeV, the only R-baryon states that are stable against strong decays are the $J = 0$ flavour singlet $\tilde{g}uds$ (S^0), the flavour octet with $J = 0$ and the lighter of the two flavour octets with $J = 1$.

We can estimate the weak-decay lifetime for $R_N \to S^0 + \pi^\pm$ to be

$$\tau_{R-N} \approx 1.6 \times 10^{-6}\,\mathrm{sec} \left(\frac{M_{\tilde{g}}}{100\,\mathrm{GeV}} \right)^2 , \tag{1}$$

by scaling the rate for $\Lambda \to N + \pi$ with particle masses as appropriate for 2-body decay kinematics. Thus, we can ignore weak decays in the rest of our analysis.

$m_{8_1} - m_{1_0}$	250 MeV
$m_{8_0} - m_{8_1}$	130 MeV

Table 2: The mass splitting of the R-baryon states stable against strong decays from [18].

The splittings between the states are summarised in Table 2[5]. In practice we can ignore many of the R-baryons. Any singly strange state in the octet can decay strongly to the flavour singlet and so should not be considered to be quasi-stable. Moreover because the R-baryons are created through interactions of the form $\tilde{\pi} + N \to \tilde{N} + \pi$ we can ignore the doubly strange states: there is no way of creating a doubly strange state from the interactions of an R-meson with the nucleons in the detector. We designate the singlet state as S^0, the spin-0 states as $\tilde{n},\ \tilde{p}$ and the spin-1 states as $\tilde{\Delta}^0,\ \tilde{\Delta}^+$.

The mass calculations of [17] and [18] were performed using several choices of bag model parameters. The primary effect of the different parameter choices is to alter the overall

[4] The R-pions are actually expected to be 40 MeV heavier than the R-rho according to [17], but this is an unnecessary level of refinement and we ignore it here.

[5] There is some uncertainty in the mass splitting that arises from the value of the zero point energy taken in the bag model calculation. We take the values in Table 2 for our model and then vary the splitting to check that our results are robust with respect to the splittings.

scale of the masses. Therefore we keep the interstate splitting within the meson and baryon sectors. We take the mass splitting between the meson and baryon sectors to be equivalent to the mass of the extra valence quark which we set to 330 MeV. In our final results we allow for this to be varied and find that this splitting has little effect on the overall conclusions.

R-baryons	
R_{uds}: S^0	$m_{\tilde{g}} + 280$ MeV
R_{8-0}: $\tilde{\Delta}^{+/0}$	$m_{\tilde{g}} + 530$ MeV
R_{8-0}: $\tilde{n}$, $\tilde{p}$	$m_{\tilde{g}} + 660$ MeV
R-mesons	
$\tilde{\pi}$	$m_{\tilde{g}} + 330$ MeV
$\tilde{K}$	$m_{\tilde{g}} + 460$ MeV

Table 3: Masses used for the R-hadrons.

Finally, we must set the overall mass normalisation with respect to the gluino mass. This value is sensitive to the details of the bag model calculations. We follow Buccella et al [18], setting $m(\tilde{n}) = m(\tilde{g}) + 660$ MeV. This fixes the overall mass scale and gives the spectrum listed in Table 3. In our final results we allow this overall scale to vary and include the effect in our estimation of the theoretical uncertainty

3 Propagation of R-hadrons through a detector

Following production in a hard collision, a gluino would largely hadronise into either an R-meson or gluino-gluon state. This particle would then be detected as it moves through a detector. In order of increasing distance from the interaction point, a typical multipurpose experiment at a collider consists of a tracker, a calorimeter and an outer muon tracker. If the R-hadron is electrically charged, its momentum would be measured in the inner and outer trackers. The energy loss of the R-hadron (hadronic and electromagnetic) would be recorded in the calorimeter.

Hadronic scattering of R-hadrons arises due to the interactions between target nucleons and the light quark system which accompanies the gluino. The much more massive gluino acts as a spectator [14]. The full list of hadronic processes we consider is given in Appendix A. For R-hadrons produced at the Tevatron the light quark system typically has $\mathcal{O}$(GeV) kinetic energy, implying that the interactions with nucleons would resemble low energy hadronic interactions. In such processes quarks can be exchanged with the quarks in the target nucleon, which can change the charge of the R-hadron. Another process in R-hadron scattering is the conversion of R-meson and gluino-gluon states to baryon states. In such processes pion production occurs. Since the pions are light these processes are exothermic and are therefore energetically favoured. Furthermore, given the absence of pions in the scattering material, the reverse process is unlikely. For the scattering model used in this work, an R-hadron experiences on average ~ 5 hadronic interactions following propagation through 2 m of iron [11], which is representative of the amount of passive material found within a typical calorimeter system at a collider experiment. This implies that most R-hadrons would be baryonic when they enter the muon detector, predominantly the spin-1 octet states R_{uud} and R_{udd} and the spin-zero singlet state S^0 (R_{uds}), as discussed in Sec. 2.

4 Simulation of R-hadrons

To simulate the R-hadron signal in the detector we employ several computer codes.

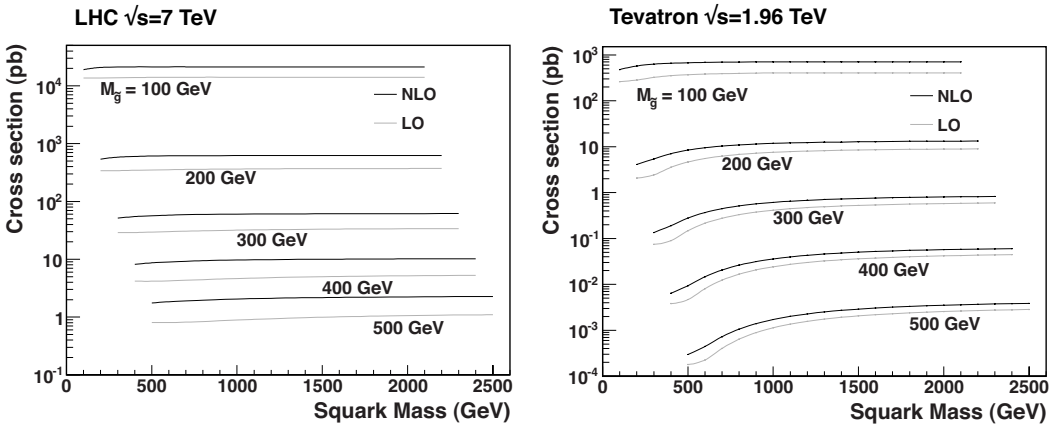

Figure 1: Gluino pair production cross section at LO and NLO shown as a function of a degenerate squark mass at five different gluino masses. The curves for the LHC are shown on the left and the Tevatron on the right

Gluino production
The cross sections for gluino pair production are calculated using Prospino2.1 [23] assuming all squarks have one degenerate mass. The cross section dependence on the squark and gluino masses is shown in Figure 1 for the Tevatron and LHC. Our limits will be based on Tevatron data, for which the lowest cross section is obtained by setting the squark mass equal to the gluino mass. Therefore we adopt equal mass squark and gluino as our standard conservative assumption and also report the gluino mass limit in the scenario where the squarks decouple; $M_{\rm sq} \gg 2M_{\tilde{g}}$. Future LHC limits on the gluino mass will be less sensitive to the assumed squark mass.

Gluino hadronization
Monte Carlo samples of the final states were generated for a $\sqrt{s} = 1.96$ TeV $p\bar{p}$ collider using Pythia [13]. The squarks and gluinos are hadronized using the same hadronization scheme as in previous studies [11, 15]. Hadronization is restricted to R-mesons only, since R-baryon production should be suppressed in a similar way that ordinary baryon production is suppressed compared to meson production. As the proportion of baryons produced compared to all particles is small in data ($< 5\%$), and we expect a similar ratio for R-baryons, we ignore the effect of direct baryon production. The gluinoball formation probability is set to 10% compared to the R-mesons.

R-hadron propagation
This sample of gluinoballs and R-mesons is then injected and propagated through the detector. For this work, a model of R-hadron scattering implemented in GEANT-4 [20] is used [15]. In view of the inherent uncertainties associated with modeling R-hadron scattering, a pragmatic approach based on analogy with observed low energy hadron scattering is adopted. The scattering rate is estimated using a constant geometric cross-section of 12 mb per light (u, d) quark and 6 mb per strange quark, all 2-to-2 and 2-to-3 processes are allowed if they are kinematically feasible, and charge conservation is respected. The proportion of 2-to-2 and 2-to-3 reactions is governed by phase space factors; no explicit constraints are applied

to the probability of baryon number exchange.

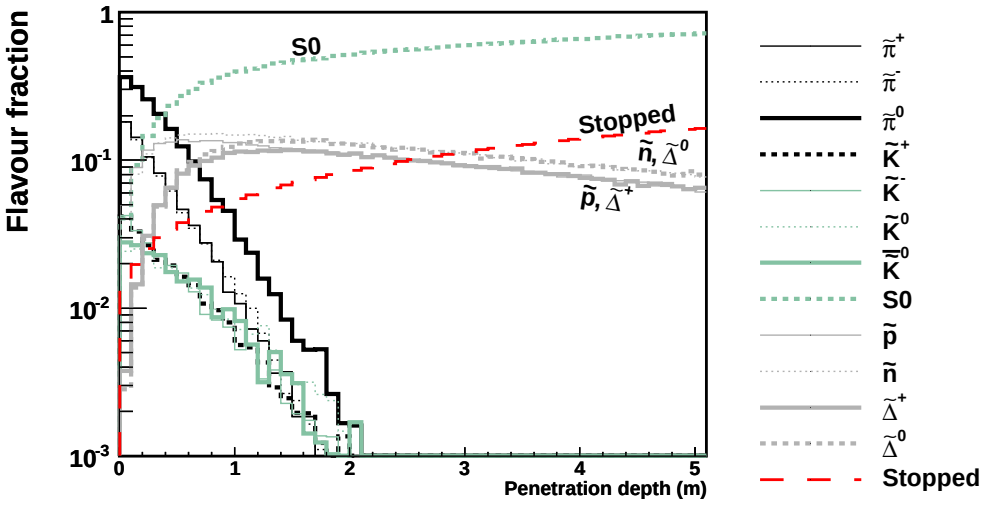

Figure 2: Flavour fractions for R-hadrons as a function of penetration depth in iron. The fractions are calculated from the percentage of gluino R-hadrons that have not stopped at the given depth. The stopping fraction is shown by the long dashed (red) line. We label the populations that are significant past 2m to aid in differentiating these lines.

Figure 2 shows the evolution of the flavour composition of an R-hadron sample for a gluino mass of 200 GeV. The kinematic distribution of the R-hadrons is taken from a Pythia event sample for this gluino mass.

5 Re-evaluating the CDF CHAMP limit for the case of meta-stable gluinos

In this section we apply the R-hadron production and propagation models developed above to obtain a limit on the mass of a quasi-stable gluino from the CDF Charge Massive Particle (CHAMP) search [6]. The CDF detector is described in detail in [12]. For the purpose of this paper, we will be focusing on the number of nuclear interaction lengths between the interaction point and the muon system. This is depicted in Figure 3. The pseudorapidity region considered in [6] is bounded by the grey dashed line.

To estimate the response of the CDF detector, the model described in Sec. 4 is supplemented with a sample of gluino R-hadrons generated with Pythia [13]. Kinematic distributions were derived from the sample, and high-statistics simulation samples were generated obeying kinematic distributions extracted from Pythia. The CDF detector was simulated using a depth of iron extracted from Figure 3 at the generated pseudorapidity. The flavour distribution of the emerging R-hadrons is shown in Figure 4.

To emulate the analysis performed in [6], only R-hadrons

- in the pseudo-rapidity interval $|\eta| < 0.7$
- in the β interval $0.4 < \beta < 0.9$

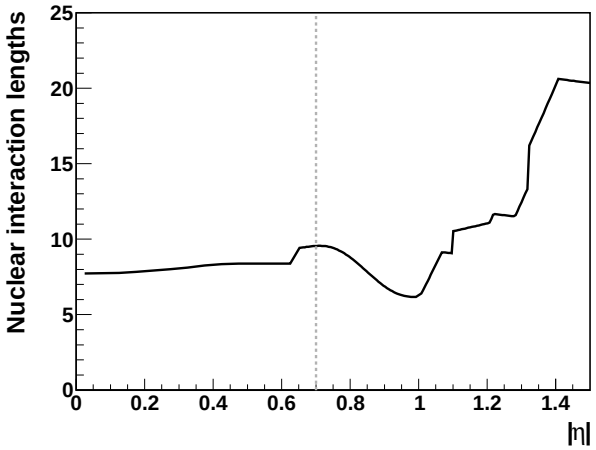

Figure 3: Matter distribution in the CDF detector as a function of pseudo-rapidity $|\eta|$.

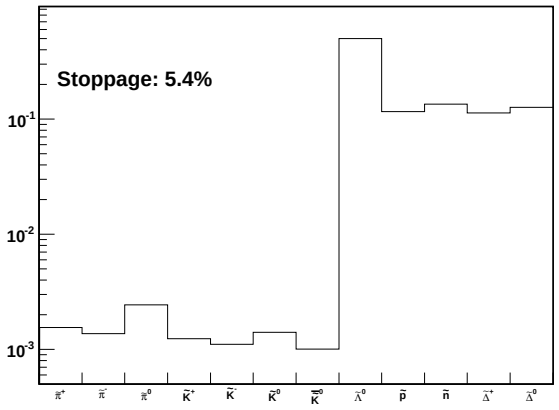

Figure 4: Flavour fractions for R-hadrons emerging from the simulated geometry.

- with a transverse momentum above 40 GeV *after traversal of the simulated iron*

were considered. Furthermore only R-hadrons that were positively charged both immediately after hadronization and after traversing the simulated geometry were considered. The probability for an R-baryon to be accepted is of order 10%. Denoting the single-object acceptance probability by x, the resulting efficiency for pair-production events to be accepted becomes

$$\epsilon_{\mathrm{Vis}} = 2x(1-x) + x^2 \tag{2}$$

yielding typical efficiencies of roughly 20%. ϵ_{Vis} is dependent upon details of the model for production, hadronisation and scattering. To check that our results are robust with respect to the theoretical uncertainty in these processes, we varied details of the model and studied the resulting change in ϵ_{Vis}. Table 4 shows ϵ_{Vis} calculated within the simulations for gluinos at four mass points. The model variations listed in the table are:

1. Increasing all R-hadron masses by 1 GeV.

Gluino mass: (GeV)	200	300	400	500
Visible Efficiency $\epsilon_{\rm Vis}$ (%)				
Base Model	20.8	18.5	15.9	13.5
1.	20.7	18.7	16.1	13.7
2.	23.6	21.3	18.5	15.7
3.	26.4	22.6	19.0	15.8
4.	18.5	16.8	14.9	12.8
5.	25.0	22.1	19.0	16.0
6.	38.0	33.2	28.1	23.5

Table 4: $\epsilon_{\rm Vis}$ for gluino pair-production events calculated at four mass points. Rows 1-6 represent variations to the base model and are described in the text.

2. Increasing the R-meson/R-baryon mass splitting by 500 MeV.
3. Setting the R-meson/R-baryon mass splitting to 0 GeV.
4. Multiplying the nuclear scattering cross section by a factor of 2
5. Multiplying the nuclear scattering cross section by a factor of 0.5
6. Using the Regge model from ref. [11] to model the nuclear scattering.

In 1-3 we explore the sensitivity of the results to uncertainty in the spectrum of R-hadron masses, while 4-6 explore the sensitivity to uncertainty in the hadronic interactions of R-hadrons. The only variation that results in a lower visible fraction arises from doubling the hadronic scattering cross-section. All other model variations result in a larger visible fraction that would give a stronger limit on the mass of the gluino than the base model we take here. Therefore we are confident that our conclusions are conservative, and robust against theoretical uncertainties.

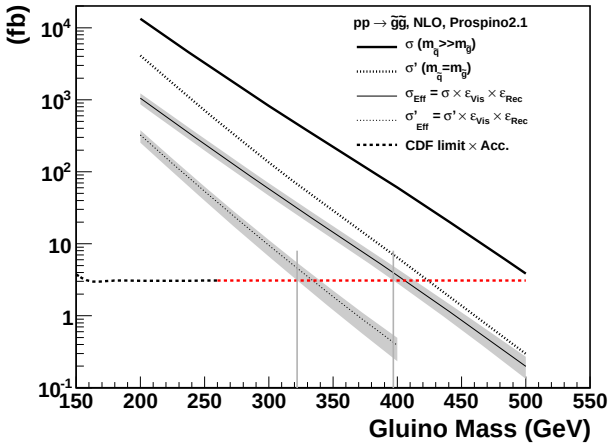

Figure 5: Calculated gluino pair production cross sections with efficiencies applied (solid and dashed lines) compared to the Tevatron limit (horizontal dashed line). We show the limit calculated for decoupled squarks (solid lines) and for squarks degenerate with the gluino (dashed lines).

The result of the simulation is shown in Figure 5. The nearly horizontal line gives CDF's 95%CL upper limit on stop squark production multiplied by the acceptance from [6]. The dependence of the acceptance on stop mass is virtually negligible, so can conservatively be extrapolated to the higher masses relevant for our limit as a constant. The red line represents a constant extrapolation. The topmost two (thick) lines are the production cross-sections for a pair of gluinos with decoupled (solid) and degenerate (dashed) squarks. These are then multiplied by the efficiency factors:

- *Acceptance* $\epsilon_{\rm Vis}$*:* The application of the nominal acceptance factors from Table 4.
- *Reconstruction efficiency* $\epsilon_{\rm Rec}$*:* A blanket reconstruction efficiency of 38 % is applied in accordance with [6].

The thin solid and dashed lines give $\sigma_{\rm Eff} = \sigma \times \epsilon_{\rm Vis} \times \epsilon_{\rm Rec}$ for decoupled and degenerate squarks respectively.

The grey bands represent the systematic uncertainties. To calculate the error the renormalization and factorization scales were increased and decreased by a factor of 2 and the standard CTEQ6 pdf [24] was replaced by the MSTW pdf [25]. The uncertainty is dominated largely by the scale variation, and the error band represents the sum in quadrature of the two sources of error. This pQCD systematic uncertainty far exceeds the uncertainties quoted in Table 4 and the latter are omitted in Figure 5.

We take the mass where the 95 %CL Tevatron limit crosses the lower error band of the effective cross section $\sigma_{\rm Eff}$ to be a lower limit on the mass of a stable gluino. This occurs at 322 GeV for the case where the squarks are degenerate with the gluino. For decoupled squarks the limit is stronger, giving a lower limit on gluino mass of 397 GeV.

6 Conclusions

We have used the results of the search for stop squark R-hadrons by CDF [6] to derive a limit on the production of a gluino-containing R-hadron and hence a lower limit on the mass of a long-lived or stable gluino. Starting from bag model predictions for the R-hadron mass spectra, we model the production, hadronisation and scattering of R-hadrons within the CDF detector and calculate the fraction of R-hadrons that mimic the signal investigated in [6]. We estimate the effects of the uncertainties in the mass spectrum, gluino production and details of the scattering model. After including systematic uncertainties, we find a lower limit of 322 GeV on the mass of a quasi-stable gluino whose mass is degenerate with squarks, and a limit of 397 GeV on the gluino mass if squarks are very massive. These are currently the strongest experimental limits on the mass of a stable or long-lived gluino and show the continued strength of Tevatron data in constraining new physics. This work also lays a foundation for interpreting future LHC searches.

Acknowledgments

This research of GRF has been supported in part by NSF-PHY-0701451. The work of JPR was supported by NSF Awards PHY-0758032, PHY-0449818 and NSF PHY-0900631, and DoE Award No. DE-FG02-06ER41417; he thanks the Niels Bohr institute for their hospitality during the completion of this work. The work of RM was supported by the Danish National Research Foundation.

References

[1] M. Fairbairn, A. C. Kraan, D. A. Milstead, T. Sjöstrand, P. Skands and T. Sloan, Phys. Rept. **438** (2007) 1 [arXiv:hep-ph/0611040].

[2] C. Amsler *et al.* [Particle Data Group Collaboration], Phys. Lett. **B667** (2008) 1.

[3] G. R. Farrar, Phys. Rev. Lett. **53** (1984) 1029.

[4] A. Heister *et al.* [ALEPH Collaboration], Eur. Phys. J. **C31** (2003) 327-342. [hep-ex/0305071].

[5] J. Abdallah *et al.* [DELPHI Collaboration], Eur. Phys. J. **C26** (2003) 505-525. [hep-ex/0303024].

[6] T. Aaltonen *et al.* [CDF Collaboration], Phys. Rev. Lett. **103** (2009) 021802. [arXiv:0902.1266 [hep-ex]].

[7] A. Aktas *et al.* [H1 Collaboration], Eur. Phys. J. **C36** (2004) 413-423. [hep-ex/0403056].

[8] V. M. Abazov *et al.* [D0 Collaboration], Phys. Rev. Lett. **102** (2009) 161802. [arXiv:0809.4472 [hep-ex]].

[9] A. C. Kraan, Eur. Phys. J. **C37** (2004) 91-104. [hep-ex/0404001].

[10] Y. R. de Boer, A. B. Kaidalov, D. A. Milstead *et al.*, J. Phys. G **G35** (2008) 075009. [arXiv:0710.3930 [hep-ph]].

[11] R. Mackeprang, D. Milstead, Eur. Phys. J. **C66** (2010) 493-501. [arXiv:0908.1868 [hep-ph]].

[12] R. Blair *et al.* [CDF-II Collaboration],

[13] T. Sjostrand, S. Mrenna and P. Z. Skands, JHEP **0605** (2006) 026 [arXiv:hep-ph/0603175].

[14] A. C. Kraan, J. B. Hansen and P. Nevski, Eur. Phys. J. C **49**, 623 (2007) [arXiv:hep-ex/0511014].

[15] R. Mackeprang and A. Rizzi, Eur. Phys. J. C **50** (2007) 353 [arXiv:hep-ph/0612161].

[16] T. A. DeGrand, R. L. Jaffe, K. Johnson and J. E. Kiskis, Phys. Rev. D **12** (1975) 2060.

[17] M. S. Chanowitz and S. R. Sharpe, Phys. Lett. B **126**, 225 (1983).

[18] F. Buccella, G. R. Farrar and A. Pugliese, Phys. Lett. B **153**, 311 (1985).

[19] M. Foster and C. Michael [UKQCD Collaboration], Phys. Rev. D **59** (1999) 094509 [arXiv:hep-lat/9811010].

[20] S. Agostinelli *et al.* [GEANT4 Collaboration], Nucl. Instrum. Meth. A **506** (2003) 250.

[21] A. Arvanitaki, S. Dimopoulos, A. Pierce, S. Rajendran and J. G. Wacker, Phys. Rev. D **76**, 055007 (2007) [arXiv:hep-ph/0506242].

[22] M. Fairbairn, A. C. Kraan, D. A. Milstead, T. Sjostrand, P. Skands and T. Sloan, Phys. Rept. **438**, 1 (2007) [arXiv:hep-ph/0611040].

[23] W. Beenakker, R. Hopker, M. Spira and P. M. Zerwas, Nucl. Phys. B **492** (1997) 51 [arXiv:hep-ph/9610490].

[24] P. M. Nadolsky *et al.*, Phys. Rev. D **78**, 013004 (2008) [arXiv:0802.0007 [hep-ph]].

[25] A. D. Martin, W. J. Stirling, R. S. Thorne and G. Watt, Eur. Phys. J. C **63**, 189 (2009) [arXiv:0901.0002 [hep-ph]].

A List of hadronic processes

This appendix contains the full process lists used in this paper. No distinction is used between R_{8-0} and R_{8-1} R-baryon states in this list, excluding processes that specifically mix the states. It is understood that any process written down for R_{8-0} particles is also valid for R_{8-1}.

$R_{uds} + N \to R_{uds} + N$
$S^0 + n \to S^0 + n$
$S^0 + p \to S^0 + p$
$R_{uds} + N \to R_{uds} + N + \pi:$
$S^0 + n \to S^0 + n + \pi^0$
$S^0 + n \to S^0 + p + \pi^-$
$S^0 + p \to S^0 + p + \pi^0$
$S^0 + p \to S^0 + n + \pi^-$
$R_{uds} + N \to R_{8-0} + K + N$
$S^0 + n \to \tilde{n} + K^0 + n$
$S^0 + n \to \tilde{n} + K^- + p$
$S^0 + n \to \tilde{p} + K^- + n$
$S^0 + p \to \tilde{p} + \bar{K}^0 + n$
$S^0 + p \to \tilde{p} + K^- + p$
$S^0 + p \to \tilde{n} + \bar{K}^0 + p$
$R_{8-0} + N \to R_{8-0} + N$
$\tilde{n} + n \to \tilde{n} + n$
$\tilde{n} + p \to \tilde{n} + p$
$\tilde{n} + p \to \tilde{p} + n$
$\tilde{p} + n \to \tilde{p} + n$
$\tilde{p} + n \to \tilde{n} + p$
$\tilde{p} + p \to \tilde{p} + p$
$R_{8-0} + N \to R_{8-0} + N + \pi$
$\tilde{n} + n \to \tilde{n} + n + \pi^0$
$\tilde{n} + n \to \tilde{n} + p + \pi^-$
$\tilde{n} + n \to \tilde{p} + n + \pi^-$
$\tilde{n} + p \to \tilde{n} + p + \pi^0$
$\tilde{n} + p \to \tilde{n} + n + \pi^+$
$\tilde{n} + p \to \tilde{p} + n + \pi^0$
$\tilde{n} + p \to \tilde{p} + p + \pi^-$
$\tilde{p} + n \to \tilde{p} + n + \pi^0$
$\tilde{p} + n \to \tilde{n} + p + \pi^0$
$\tilde{p} + n \to \tilde{n} + n + \pi^+$
$\tilde{p} + n \to \tilde{p} + p + \pi^-$
$\tilde{p} + p \to \tilde{p} + p + \pi^0$
$\tilde{p} + p \to \tilde{p} + n + \pi^+$
$\tilde{p} + p \to \tilde{n} + p + \pi^+$

$R_{8-0} + N \to R_{8-1} + N$
$\tilde{n} + n \to \tilde{\Delta}^0 + n$
$\tilde{n} + p \to \tilde{\Delta}^0 + p$
$\tilde{n} + p \to \tilde{\Delta}^+ + n$
$\tilde{p} + n \to \tilde{\Delta}^+ + n$
$\tilde{p} + n \to \tilde{\Delta}^0 + p$
$\tilde{p} + p \to \tilde{\Delta}^+ + p$
$R_{8-0} + N \to R_{8-1} + N + \pi$
$\tilde{n} + n \to \tilde{\Delta}^0 + n + \pi^0$
$\tilde{n} + n \to \tilde{\Delta}^0 + p + \pi^-$
$\tilde{n} + n \to \tilde{\Delta}^+ + n + \pi^-$
$\tilde{n} + p \to \tilde{\Delta}^0 + p + \pi^0$
$\tilde{n} + p \to \tilde{\Delta}^0 + n + \pi^+$
$\tilde{n} + p \to \tilde{\Delta}^+ + n + \pi^0$
$\tilde{n} + p \to \tilde{\Delta}^+ + p + \pi^-$
$\tilde{p} + n \to \tilde{\Delta}^+ + n + \pi^0$
$\tilde{p} + n \to \tilde{\Delta}^0 + p + \pi^0$
$\tilde{p} + n \to \tilde{\Delta}^0 + n + \pi^+$
$\tilde{p} + n \to \tilde{\Delta}^+ + p + \pi^-$
$\tilde{p} + p \to \tilde{\Delta}^+ + p + \pi^0$
$\tilde{p} + p \to \tilde{\Delta}^+ + n + \pi^+$
$\tilde{p} + p \to \tilde{\Delta}^0 + p + \pi^+$
$R_{8-0} + N \to R_{uds} + K + N$
$\tilde{n} + n \to S^0 + K^0 + n$
$\tilde{n} + p \to S^0 + K^0 + p$
$\tilde{n} + p \to S^0 + K^+ + n$
$\tilde{p} + n \to S^0 + K^0 + p$
$\tilde{p} + n \to S^0 + K^+ + n$
$\tilde{p} + p \to S^0 + K^+ + p$

Table 5: Process lists galore for baryons

$\tilde{\pi} + N \to \tilde{\pi} + N$
$\tilde{\pi}^0 + n \to \tilde{\pi}^0 + n$
$\tilde{\pi}^0 + n \to \tilde{\pi}^- + p$
$\tilde{\pi}^0 + p \to \tilde{\pi}^0 + p$
$\tilde{\pi}^0 + p \to \tilde{\pi}^+ + n$
$\tilde{\pi}^- + n \to \tilde{\pi}^- + n$
$\tilde{\pi}^- + p \to \tilde{\pi}^- + p$
$\tilde{\pi}^- + p \to \tilde{\pi}^0 + n$
$\tilde{\pi}^+ + n \to \tilde{\pi}^+ + n$
$\tilde{\pi}^+ + n \to \tilde{\pi}^0 + p$
$\tilde{\pi}^+ + p \to \tilde{\pi}^+ + p$
$\tilde{\pi} + N \to \tilde{\pi} + N + \pi$
$\tilde{\pi}^0 + n \to \tilde{\pi}^0 + n + \pi^0$
$\tilde{\pi}^0 + n \to \tilde{\pi}^0 + p + \pi^-$
$\tilde{\pi}^0 + n \to \tilde{\pi}^+ + n + \pi^-$
$\tilde{\pi}^0 + n \to \tilde{\pi}^- + p + \pi^0$
$\tilde{\pi}^0 + n \to \tilde{\pi}^- + n + \pi^+$
$\tilde{\pi}^0 + p \to \tilde{\pi}^0 + p + \pi^0$
$\tilde{\pi}^0 + p \to \tilde{\pi}^0 + n + \pi^+$
$\tilde{\pi}^0 + p \to \tilde{\pi}^+ + n + \pi^0$
$\tilde{\pi}^0 + p \to \tilde{\pi}^+ + p + \pi^-$
$\tilde{\pi}^0 + p \to \tilde{\pi}^- + p + \pi^+$
$\tilde{\pi} + N \to R_{8-0} + \pi$
$\tilde{\pi}^0 + n \to \tilde{n} + \pi^0$
$\tilde{\pi}^0 + n \to \tilde{p} + \pi^-$
$\tilde{\pi}^0 + p \to \tilde{n} + \pi^+$
$\tilde{\pi}^0 + p \to \tilde{p} + \pi^0$
$\tilde{\pi}^+ + n \to \tilde{p} + \pi^0$
$\tilde{\pi}^+ + n \to \tilde{n} + \pi^+$
$\tilde{\pi}^+ + p \to \tilde{p} + \pi^+$
$\tilde{\pi}^- + n \to \tilde{n} + \pi^-$
$\tilde{\pi}^- + p \to \tilde{n} + \pi^0$
$\tilde{\pi}^- + p \to \tilde{p} + \pi^-$

$\tilde{\pi} + N \to R_{8-0} + \pi + \pi$
$\tilde{\pi}^0 + n \to \tilde{n} + \pi^0 + \pi^0$
$\tilde{\pi}^0 + n \to \tilde{n} + \pi^+ + \pi^-$
$\tilde{\pi}^0 + n \to \tilde{p} + \pi^- + \pi^0$
$\tilde{\pi}^0 + p \to \tilde{n} + \pi^+ + \pi^0$
$\tilde{\pi}^0 + p \to \tilde{p} + \pi^0 + \pi^0$
$\tilde{\pi}^0 + p \to \tilde{p} + \pi^+ + \pi^-$
$\tilde{\pi}^+ + n \to \tilde{p} + \pi^0 + \pi^0$
$\tilde{\pi}^+ + n \to \tilde{p} + \pi^+ + \pi^-$
$\tilde{\pi}^+ + n \to \tilde{n} + \pi^+ + \pi^0$
$\tilde{\pi}^+ + p \to \tilde{p} + \pi^+ + \pi^-$
$\tilde{\pi}^+ + p \to \tilde{n} + \pi^+ + \pi^+$
$\tilde{\pi}^- + n \to \tilde{n} + \pi^- + \pi^0$
$\tilde{\pi}^- + n \to \tilde{p} + \pi^- + \pi^-$
$\tilde{\pi}^- + p \to \tilde{n} + \pi^0 + \pi^0$
$\tilde{\pi}^- + p \to \tilde{n} + \pi^+ + \pi^-$
$\tilde{\pi}^- + p \to \tilde{p} + \pi^- + \pi^0$
$\tilde{\pi} + N \to R_{uds} + K$
$\tilde{\pi}^0 + n \to S^0 + K^0$
$\tilde{\pi}^0 + p \to S^0 + K^+$
$\tilde{\pi}^+ + n \to S^0 + K^+$
$\tilde{\pi}^- + p \to S^0 + K^0$
$\tilde{\pi} + N \to R_{uds} + K + \pi$
$\tilde{\pi}^0 + n \to S^0 + K^0 + \pi^0$
$\tilde{\pi}^0 + n \to S^0 + K^+ + \pi^-$
$\tilde{\pi}^0 + p \to S^0 + K^+ + \pi^0$
$\tilde{\pi}^0 + p \to S^0 + K^0 + \pi^+$
$\tilde{\pi}^+ + n \to S^0 + K^+ + \pi^0$
$\tilde{\pi}^+ + n \to S^0 + K^0 + \pi^+$
$\tilde{\pi}^+ + p \to S^0 + K^+ + \pi^+$
$\tilde{\pi}^- + n \to S^0 + K^0 + \pi^-$
$\tilde{\pi}^- + p \to S^0 + K^0 + \pi^0$
$\tilde{\pi}^- + p \to S^0 + K^+ + \pi^-$

$\tilde{K} + N \to \tilde{K} + N$
$\tilde{K}^+ + n \to \tilde{K}^+ + n$
$\tilde{K}^+ + n \to \tilde{K}^0 + p$
$\tilde{K}^+ + p \to \tilde{K}^+ + p$
$\tilde{K}^- + n \to \tilde{K}^- + n$
$\tilde{K}^- + p \to \tilde{K}^- + p$
$\tilde{K}^- + p \to \bar{\tilde{K}}^0 + n$
$\tilde{K}^0 + n \to \tilde{K}^0 + n$
$\tilde{K}^0 + p \to \tilde{K}^0 + p$
$\tilde{K}^0 + p \to \tilde{K}^+ + n$
$\bar{\tilde{K}}^0 + n \to \bar{\tilde{K}}^0 + n$
$\bar{\tilde{K}}^0 + n \to \tilde{K}^- + p$
$\bar{\tilde{K}}^0 + p \to \bar{\tilde{K}}^0 + p$
$\tilde{K} + N \to \tilde{K} + N + \pi$
$\tilde{K}^+ + n \to \tilde{K}^+ + n + \pi^0$
$\tilde{K}^+ + n \to \tilde{K}^0 + p + \pi^0$
$\tilde{K}^+ + n \to \tilde{K}^0 + n + \pi^+$
$\tilde{K}^+ + n \to \tilde{K}^+ + p + \pi^-$
$\tilde{K}^+ + p \to \tilde{K}^+ + p + \pi^0$
$\tilde{K}^+ + p \to \tilde{K}^+ + n + \pi^+$
$\tilde{K}^+ + p \to \tilde{K}^0 + p + \pi^+$
$\tilde{K}^- + n \to \tilde{K}^- + n + \pi^0$
$\tilde{K}^- + n \to \tilde{K}^- + p + \pi^-$
$\tilde{K}^- + n \to \bar{\tilde{K}}^0 + n + \pi^-$
$\tilde{K}^- + p \to \tilde{K}^- + p + \pi^0$
$\tilde{K}^- + p \to \tilde{K}^- + n + \pi^+$
$\tilde{K}^- + p \to \bar{\tilde{K}}^0 + n + \pi^0$
$\tilde{K}^- + p \to \bar{\tilde{K}}^0 + p + \pi^-$
$\tilde{K}^0 + n \to \tilde{K}^0 + n + \pi^0$
$\tilde{K}^0 + n \to \tilde{K}^0 + p + \pi^-$
$\tilde{K}^0 + n \to \tilde{K}^+ + n + \pi^-$
$\tilde{K}^0 + p \to \tilde{K}^0 + p + \pi^0$
$\tilde{K}^0 + p \to \tilde{K}^0 + n + \pi^+$
$\tilde{K}^0 + p \to \tilde{K}^+ + n + \pi^0$
$\tilde{K}^0 + p \to \tilde{K}^+ + p + \pi^-$
$\bar{\tilde{K}}^0 + n \to \bar{\tilde{K}}^0 + n + \pi^0$
$\bar{\tilde{K}}^0 + n \to \bar{\tilde{K}}^0 + p + \pi^-$
$\bar{\tilde{K}}^0 + n \to \tilde{K}^- + p + \pi^0$
$\bar{\tilde{K}}^0 + n \to \tilde{K}^- + n + \pi^+$
$\bar{\tilde{K}}^0 + p \to \bar{\tilde{K}}^0 + p + \pi^0$
$\bar{\tilde{K}}^0 + p \to \bar{\tilde{K}}^0 + n + \pi^+$
$\bar{\tilde{K}}^0 + p \to \tilde{K}^- + p + \pi^+$

Table 6: Process lists galore for mesons

$\tilde{K} + N \to R_{uds} + \pi$
$\tilde{K}^- + n \to S^0 + \pi^-$
$\tilde{K}^- + p \to S^0 + \pi^0$
$\bar{\tilde{K}}^0 + n \to S^0 + \pi^0$
$\bar{\tilde{K}}^0 + p \to S^0 + \pi^+$
$\tilde{K} + N \to R_{uds} + \pi + \pi$
$\tilde{K}^- + n \to S^0 + \pi^- + \pi^0$
$\tilde{K}^- + p \to S^0 + \pi^0 + \pi^0$
$\tilde{K}^- + p \to S^0 + \pi^+ + \pi^-$
$\bar{\tilde{K}}^0 + n \to S^0 + \pi^0 + \pi^0$
$\bar{\tilde{K}}^0 + n \to S^0 + \pi^+ + \pi^-$
$\bar{\tilde{K}}^0 + p \to S^0 + \pi^+ + \pi^0$
$\tilde{K} + N \to R_{8-0} + K$
$\tilde{K}^+ + n \to \tilde{n} + K^+$
$\tilde{K}^+ + n \to \tilde{p} + K^0$
$\tilde{K}^+ + p \to \tilde{p} + K^+$
$\tilde{K}^+ + p \to \tilde{n} + K^0$
$\tilde{K}^- + n \to \tilde{n} + K^-$
$\tilde{K}^- + p \to \tilde{p} + K^-$
$\tilde{K}^- + p \to \tilde{n} + \bar{K}^0$
$\tilde{K}^0 + n \to \tilde{n} + K^0$
$\tilde{K}^0 + p \to \tilde{p} + K^0$
$\tilde{K}^0 + p \to \tilde{n} + K^+$
$\bar{\tilde{K}}^0 + n \to \tilde{n} + \bar{K}^0$
$\bar{\tilde{K}}^0 + n \to \tilde{p} + K^-$
$\bar{\tilde{K}}^0 + p \to \tilde{p} + \bar{K}^0$

$\tilde{K} + N \to R_{8-0} + K + \pi$
$\tilde{K}^+ + n \to \tilde{n} + K^+ + \pi^0$
$\tilde{K}^+ + n \to \tilde{n} + K^0 + \pi^+$
$\tilde{K}^+ + n \to \tilde{p} + K^0 + \pi^0$
$\tilde{K}^+ + n \to \tilde{p} + K^+ + \pi^-$
$\tilde{K}^+ + p \to \tilde{p} + K^+ + \pi^0$
$\tilde{K}^+ + p \to \tilde{p} + K^0 + \pi^+$
$\tilde{K}^+ + p \to \tilde{n} + K^+ + \pi^+$
$\tilde{K}^- + n \to \tilde{n} + K^- + \pi^0$
$\tilde{K}^- + n \to \tilde{n} + \bar{K}^0 + \pi^-$
$\tilde{K}^- + n \to \tilde{p} + K^- + \pi^-$
$\tilde{K}^- + p \to \tilde{p} + K^- + \pi^0$
$\tilde{K}^- + p \to \tilde{p} + \bar{K}^0 + \pi^-$
$\tilde{K}^- + p \to \tilde{n} + \bar{K}^0 + \pi^0$
$\tilde{K}^- + p \to \tilde{n} + K^- + \pi^+$
$\bar{\tilde{K}}^0 + n \to \tilde{n} + \bar{K}^0 + \pi^0$
$\bar{\tilde{K}}^0 + n \to \tilde{n} + K^- + \pi^+$
$\bar{\tilde{K}}^0 + n \to \tilde{p} + K^- + \pi^0$
$\bar{\tilde{K}}^0 + n \to \tilde{p} + \bar{K}^0 + \pi^-$
$\bar{\tilde{K}}^0 + p \to \tilde{p} + \bar{K}^0 + \pi^0$
$\bar{\tilde{K}}^0 + p \to \tilde{p} + K^- + \pi^+$
$\bar{\tilde{K}}^0 + p \to \tilde{n} + \bar{K}^0 + \pi^+$
$\tilde{K}^0 + n \to \tilde{n} + K^- + \pi^0$
$\tilde{K}^0 + n \to \tilde{n} + \bar{K}^0 + \pi^-$
$\tilde{K}^0 + n \to \tilde{p} + K^- + \pi^-$
$\tilde{K}^0 + p \to \tilde{p} + K^- + \pi^0$
$\tilde{K}^0 + p \to \tilde{p} + \bar{K}^0 + \pi^-$
$\tilde{K}^0 + p \to \tilde{n} + \bar{K}^0 + \pi^0$
$\tilde{K}^0 + p \to \tilde{n} + K^- + \pi^+$

Table 7: Baryon number changing processes for strange mesons